Calculation of thermodynamic and mechanical properties of silicon nanostructures using the local phonon density of states

Z. Tang and N. R. Aluru

Department of Mechanical Science and Engineering, Beckman Institute for Advanced Science and Technology, University of Illinois at Urbana-Champaign, Urbana, Illinois 61801, USA

(Received 28 August 2006; revised manuscript received 30 October 2006; published 27 December 2006)

We investigate thermodynamic and mechanical properties of silicon nanostructures at finite temperature. Thermodynamic properties for finite-temperature solid systems under isothermal conditions are characterized by the Helmholtz free energy density. The static part of the Helmholtz free energy is obtained directly from the interatomic potential, while the vibrational part is calculated by using the theory of local phonon density of states (LPDOS). The LPDOS is calculated efficiently from the on-site phonon Green's function by using a recursion technique based on a continued fraction representation. The Cauchy-Born hypothesis is employed to compute the mechanical properties. By considering ideal Si{001}, (2×1) reconstructed Si{001}, and monolayer-hydrogen-passivated (2×1) reconstructed Si{001} surfaces of a silicon nanowire, we calculate the local phonon structure and local thermodynamic and mechanical properties at finite temperature and observe that the surface effects on the local thermal and mechanical properties are localized to within one or two atomic layers of the silicon nanowire.

DOI: 10.1103/PhysRevB.74.235441 PACS number(s): 63.22.+m, 68.35.Md, 62.25.+g, 02.70.−c

I. INTRODUCTION

In recent years, silicon nanostructures have attracted considerable attention due to their potential applications in nanoelectromechanical, nanoelectronic, and optoelectronic devices.[1–3] The calculation of thermodynamic and mechanical properties of silicon nanostructures plays an important role in developing the physical theories and computational design tools that describe the motion and operation of silicon nanodevices.[4] First-principles quantum mechanical methods are generally most accurate for predicting the material properties. *Ab initio* local density functional techniques have been used to determine the thermodynamic properties of silicon.[5] However, due to the complexity of these methods and the need for large computational resources, *ab initio* calculations are limited to very small systems. Empirical and semiempirical interatomic potentials[6,7] have been developed to provide a simpler and yet a reasonably accurate description of materials. Classical molecular dynamics (MD) and Monte Carlo (MC) simulation are two popular methods that are based on interatomic potentials. In these methods, the phonon density of states can be calculated by the Fourier transform of the velocity-autocorrelation function.[8] Once the phonon structures are known, the thermodynamic properties can be easily computed. Despite their popularity, computational cost is still an inherent drawback with the MD and the MC methods. In addition, in these methods, it is also difficult to calculate the mechanical properties, where the derivatives of the thermodynamic properties with respect to the deformation parameters are needed, due to the stochastic behavior of the atom velocities. Another class of methods rely on the theory of quantum-mechanical lattice dynamics and these methods are an attractive alternative for computational analysis of material properties. The key step in the lattice dynamics approach is the quasiharmonic approximation of the interatomic potential.[9] For a system of N atoms with a given interatomic potential, Helmholtz free energy and other thermodynamic properties can be computed by diagonalizing a $3N\times3N$ force constant matrix.[9] Alternative approaches such as the local quasiharmonic method[10] (LQHM) and the quasiharmonic approximation in the reciprocal space[9] (QHMK) have also been proposed. As a simplification of the quasiharmonic approximation, the LQHM reduces the $3N\times3N$ eigenvalue problem to N 3×3 eigenvalue problems. The LQHM, however, neglects the coupling between the vibrations of different atoms and this can result in errors.[11,12] The QHMK relies on a periodic boundary condition and can be accurate and efficient for bulk silicon structures. However, the use of periodic boundary conditions can be inaccurate for nanostructures (with a finite number of atoms along a particular direction) and this can result in errors for confined silicon nanostructures.

In this paper, a quasiharmonic approximation with phonon Green's function (QHMG) approach—where the quasiharmonic approximation is combined with the local phonon density of states (LPDOS)—is developed to compute the local phonon structures,[13–15] and thermodynamic and mechanical properties of silicon nanostructures. The LPDOS is efficiently calculated from the phonon Green's function (GF) by using a recursion method. The mechanical properties are calculated by using the Cauchy-Born rule[16] within the quasicontinuum framework.[17] We show that the QHMG approach can be an accurate and an efficient way to determine the local thermal and mechanical properties of nanostructures at finite temperature.

The rest of the paper is organized as follows: in Sec. II, the theory of lattice dynamics, LPDOS, phonon GF, recursion method, local thermodynamic properties, and local mechanical properties are introduced; in Sec. III, different silicon surface models and the empirical interatomic potential models are introduced; in Sec. IV, we compute the phonon structures, thermal properties, and mechanical properties of silicon nanowires; and conclusions are given in Sec. V.

II. THEORY

A. Lattice dynamics

The most commonly used method to compute the thermodynamic properties of crystals is the lattice dynamics theory based on the quasiharmonic approximation.[18] Considering an N-atom system, the total potential energy is first expanded using a Taylor's series expansion. In a quasiharmonic approximation, the higher-order (>2) terms are neglected and the total potential energy can thus be written in a quadratic form,

$$U(\mathbf{x}) = U(\mathbf{x}^0) + \frac{1}{2}\sum_{\alpha,\beta=1}^{N}\sum_{j,k=1}^{3}\left.\frac{\partial^2 U(\mathbf{x})}{\partial x_{\alpha j}\partial x_{\beta k}}\right|_{\mathbf{x}=\mathbf{x}^0}(x_{\alpha j}-x_{\alpha j}^0)(x_{\beta k}-x_{\beta k}^0), \tag{1}$$

where $\mathbf{x}$ denotes the instantaneous position of all the atoms in the system, i.e., $\mathbf{x}=(\mathbf{x}_1,\mathbf{x}_2,\ldots,\mathbf{x}_N)$, $\mathbf{x}^0$ denotes the equilibrium position of all the atoms in the system, i.e., $\mathbf{x}^0=(\mathbf{x}_1^0,\mathbf{x}_2^0,\ldots,\mathbf{x}_N^0)$, $\mathbf{x}_\alpha$ and $\mathbf{x}_\alpha^0$ are the instantaneous and equilibrium position vectors of atom α, $\alpha=1,2,\ldots,N$, respectively, $x_{\alpha j}$ and $x_{\beta k}$ are the components of the position vectors $\mathbf{x}_\alpha$ and $\mathbf{x}_\beta$ along the jth and kth directions, respectively, and $x_{\alpha j}^0$ and $x_{\beta k}^0$ are the components of the position vectors $\mathbf{x}_\alpha^0$ and $\mathbf{x}_\beta^0$ along the jth and kth directions, respectively. The elements of the $3N\times 3N$ force constant matrix Φ, are defined as

$$\Phi_{3\alpha-3+j,3\beta-3+k} = \left.\frac{\partial^2 U(\mathbf{x})}{\partial x_{\alpha j}\partial x_{\beta k}}\right|_{\mathbf{x}=\mathbf{x}^0}, \tag{2}$$

$$\alpha,\beta = 1,2,\ldots,N, \quad j,k = 1,2,3.$$

Furthermore, a mass-weighted force constant matrix can be defined by

$$\hat{\Phi}_{3\alpha-3+j,3\beta-3+k} = \frac{1}{\sqrt{M_\alpha M_\beta}}\Phi_{3\alpha-3+j,3\beta-3+k}, \tag{3}$$

$$\alpha,\beta = 1,2,\ldots,N, \quad j,k = 1,2,3,$$

where M_α and M_β are the masses of atoms α and β, respectively. In the theory of lattice dynamics, the phonon frequencies can be calculated from the eigenvalues of the mass-weighted force constant matrix, i.e., $\omega_l=\sqrt{\lambda^{(l)}}$, $l=1,2,\ldots,3N$, where ω_l is the lth phonon frequency, and $\lambda^{(l)}$ is the lth eigenvalue of $\hat{\Phi}$. Once the phonon frequencies are known, the Helmholtz free energy, A, for an N-atom system is given by[16]

$$A = U(\mathbf{x}^0) + k_B T\sum_{l=1}^{3N}\ln\left[2\sinh\left(\frac{\hbar\omega_l}{2k_B T}\right)\right], \tag{4}$$

where the first term $U(\mathbf{x}^0)$ on the right-hand side is the static potential energy, the second term is the vibrational energy, k_B is the Boltzmann constant, T is the temperature, and $\hbar$ is the reduced Planck's constant.

B. LPDOS and local thermodynamic properties

The Helmholtz free energy A computed by Eq. (4), is a global property of the system. To compute the local thermodynamic properties of a system, a useful and an important quantity is the LPDOS,[9,19] which is defined as

$$n(\omega,\mathbf{x}_\alpha) = \sum_{j=1}^{3}\sum_{l=1}^{3N}\delta(\omega-\omega_l)|\psi_l(x_{\alpha j})|^2, \quad \alpha = 1,2,\ldots,N, \tag{5}$$

where $\psi_l(x_{\alpha j})$ is the element of the eigenvector corresponding to ω_l at position $x_{\alpha j}$, and ω is the phonon frequency. Using the definition of LPDOS, the Helmholtz free energy A in Eq. (4) can be rewritten as[9]

$$A_\alpha = U_\alpha + k_B T\int_0^{\omega_{\max}}\ln\left(2\sinh\frac{\hbar\omega}{2k_B T}\right)n(\omega,\mathbf{x}_\alpha)d\omega, \tag{6}$$

where A_α and U_α are the Helmholtz free energy and the static potential energy of atom α, respectively, and $\omega_{\max}$ is the maximum phonon frequency. The total Helmholtz free energy $A=\Sigma_{\alpha=1}^{N}A_\alpha$. Other thermodynamic quantities can be easily derived once the Helmholtz free energy is known.[20] For example, the local internal energy of atom α is given by $E_\alpha=A_\alpha-T(\partial A_\alpha/\partial T)$, the local heat capacity of an atom α is given by $C_{v\alpha}=-T(\partial^2 A_\alpha/\partial T^2)$, and the local entropy of an atom α is given by $S_\alpha=(E_\alpha-A_\alpha)/T$.

C. Phonon GF and the recursion method

The calculation of LPDOS by Eq. (5) requires that all the phonon frequencies ω_l, $l=1,2,\ldots,3N$, are known. The calculation of all the phonon frequencies of the system can be quite expensive. An alternative approach is to calculate the LPDOS by using the phonon GF. In this section, the LPDOS is first related to the phonon GF.[21] Then an efficient numerical scheme, the recursion method,[13–15] is used to calculate the phonon GF and LPDOS.

The general intersite phonon GF is given by[21]

$$G_{\alpha j,\beta k}(\omega^2) = [(\omega^2\mathbf{I}-\hat{\Phi})^{-1}]_{3\alpha-3+j,3\beta-3+k} = \sum_{l=1}^{3N}\frac{\psi_l(x_{\alpha j})\psi_l^\dagger(x_{\beta k})}{\omega^2-\omega_l^2}, \tag{7}$$

$$\alpha,\beta = 1,2,\ldots,N, \quad j,k = 1,2,3,$$

where the combination αj denotes the row index $3\alpha-3+j$, and the combination βk denotes the column index $3\beta-3+k$ of the $3N\times 3N$ matrix $G(\omega^2)$, ω is the frequency, $\mathbf{I}$ is the identity matrix, and $\psi_l^\dagger(x_{\beta k})$ is the complex conjugate of $\psi_l(x_{\beta k})$. When $\omega=\omega_l$, the phonon GF in Eq. (7) is defined by a limiting procedure,[21] i.e.,

$$\lim_{\epsilon\to 0^+}G_{\alpha j,\beta k}(\omega^2+i\epsilon) = \lim_{\epsilon\to 0^+}\sum_{l=1}^{3N}\frac{\psi_l(x_{\alpha j})\psi_l^\dagger(x_{\beta k})}{\omega^2-\omega_l^2+i\epsilon}. \tag{8}$$

By using the identities for the δ function,

$$\delta(\omega^2-\omega_l^2) = -\frac{1}{\pi}\lim_{\epsilon\to 0^+}\mathrm{Im}\frac{1}{\omega^2-\omega_l^2+i\epsilon}, \tag{9}$$

$$\delta(\omega^2 - \omega_l^2) = \frac{1}{2\omega}\delta(\omega - \omega_l), \tag{10}$$

the diagonal entries of the phonon GF matrix $G(\omega^2)$ can be written as

$$2\omega\left(-\frac{1}{\pi}\lim_{\epsilon\to 0^+}\mathrm{Im}\, G_{\alpha j,\alpha j}(\omega^2 + i\epsilon)\right) = \sum_{l=1}^{3N}\delta(\omega - \omega_l)|\psi_l(x_{\alpha j})|^2. \tag{11}$$

By comparing Eqs. (5) and (11), the LPDOS for an atom α can be calculated from the on-site phonon GFs [on-site phonon GFs refer to the diagonal entries of the $3N\times 3N$ phonon GF matrix $G(\omega^2)$] by[21]

$$n(\omega, \mathbf{x}_\alpha) = 2\omega\left(-\frac{1}{\pi}\lim_{\epsilon\to 0^+}\mathrm{Im}\sum_{j=1}^{3} G_{\alpha j,\alpha j}(\omega^2 + i\epsilon)\right), \tag{12}$$

where $\mathrm{Im}\,\Sigma_{j=1}^{3} G_{\alpha j,\alpha j}$ represents the imaginary part of the summation of the on-site phonon GFs for atom α.

To compute the LPDOS by using Eq. (12), only the diagonal entries of the phonon GF matrix are needed. The direct matrix inversion in Eq. (7) [i.e., $G(\omega^2)=(\omega^2\mathbf{I}-\hat{\Phi})^{-1}$] to compute the diagonal entries of $G(\omega^2)$ is numerically very expensive. If the mass-weighted force constant matrix $\hat{\Phi}$ is diagonal, the diagonal entries of the phonon GF matrix can be easily obtained. However, the process of diagonalizing the mass-weighted force constant matrix is also computationally expensive when the dimension of $\hat{\Phi}$ is large. As an alternative method, if the mass-weighted force constant matrix can be transformed into a tridiagonal form, then the diagonal entries of the phonon GF can be easily obtained. Note that, if the mass-weighted force constant matrix $\hat{\Phi}$ is symmetric, the tridiagonalized force constant matrix Φ^{TD} obtained by using orthogonal transformation matrices, will also be symmetric. Expressing Φ^{TD} as

$$\Phi^{TD} = \begin{bmatrix} a_1 & b_2 & & & \\ b_2 & a_2 & b_3 & & \\ & \ddots & \ddots & \ddots & \\ & & b_{3N-1} & a_{3N-1} & b_{3N} \\ & & & b_{3N} & a_{3N} \end{bmatrix}, \tag{13}$$

the modified GF matrix using Φ^{TD} is given by

$$\tilde{G}(Z) = (Z\mathbf{I} - \Phi^{TD})^{-1}, \tag{14}$$

where $Z=\omega^2+i\epsilon$. By using the symmetric and tridiagonal properties of Φ^{TD}, the entries of $\tilde{G}(Z)$ can be represented as continued fractions.[22] For example, the first diagonal entry of $\tilde{G}(Z)$ is given by

$$\tilde{G}_{11}(Z) = \cfrac{1}{Z - a_1 - \cfrac{b_2^2}{Z - a_2 - \cfrac{b_3^2}{\ddots \cfrac{b_{3N}^2}{Z - a_{3N}}}}}. \tag{15}$$

Denoting L to be the orthogonal transformation matrix used to construct Φ^{TD}, the relation between $G(Z)$ and $\tilde{G}(Z)$ is given by

$$G(Z) = L\tilde{G}(Z)L^T. \tag{16}$$

The calculation of all the diagonal and the off-diagonal elements of the tridiagonalized force constant matrix Φ^{TD} can still be expensive, i.e., $O(N^2)$ computational cost.[23] The convergence property of the coefficients a_l, $l=1,\ldots,3N$, and b_l, $l=2,\ldots,3N$, allows that one can compute the first n-level coefficients (n being far less than $3N$) and approximate all the high order coefficients as a_∞ and b_∞. Based on this approximation, the continued fraction in Eq. (15) is calculated exactly up to n levels and the rest of the continued fraction is approximated by an infinite level continued fraction, i.e., $\tilde{G}_{11}(Z)$ can be rewritten as

$$\tilde{G}_{11}(Z) = \cfrac{1}{Z - a_1 - \cfrac{b_2^2}{Z - a_2 - \cfrac{b_3^2}{\ddots \cfrac{b_n^2}{Z - a_n - b_{n+1}^2 t(Z)}}}}, \tag{17}$$

where $t(Z)$ is defined as the square root terminator (SRT) function[24] and is given by

$$t(Z) = \frac{1}{b_\infty}[\eta(Z) - i\sqrt{1-\eta^2(Z)}], \tag{18}$$

i is the complex number, and $\eta(Z)=(Z-a_\infty)/2b_\infty$. The terminating coefficients a_∞ and b_∞ need to be computed appropriately as the higher order coefficients represent less local and more distant structural information. Although the higher-order coefficients can be predicted by an extrapolation technique,[25] in our work, we choose a_∞ and b_∞ by averaging over the first n levels, i.e., $a_\infty=(1/n)\Sigma_{l=1}^{n} a_l$, $b_\infty=(1/n)\Sigma_{l=2}^{n+1} b_l$.

The tridiagonalization of the mass-weighted force constant matrix can be realized by using the Lanczos algorithm.[26] In the numerical scheme, for a given atom index α and a direction index j (i.e., to compute $G_{\alpha j,\alpha j}$), the starting Lanczos state is set as

$$\phi_1 = (\ldots,0,1,0,\ldots)^T \tag{19}$$

where the only nonzero entry is located in the $(3\alpha-3+j)$th position. We also set $b_1=0$, $\phi_0=\mathbf{0}$, and we can compute a_1 as $a_1=\phi_1^T\hat{\Phi}\phi_1$. The Lanczos recursion relation for the mass-

weighted force constant matrix $\hat{\Phi}$ applied to a sequence of vectors,

$$\tilde{\phi}_{l+1} = (\hat{\Phi} - a_l \mathbf{I})\phi_l - b_l \phi_{l-1}, \quad l = 1,2,\ldots,n-1, \quad (20)$$

generates the recursion coefficients (RCs), $a_{l+1} = \tilde{\phi}_{l+1}^T \hat{\Phi} \tilde{\phi}_{l+1}$, $b_{l+1} = \sqrt{\tilde{\phi}_{l+1}^T \tilde{\phi}_{l+1}}$, and the set of normalized vectors $\phi_{l+1} = \tilde{\phi}_{l+1}/b_{l+1}$, $l=1,2,\ldots,n-1$. From the Lanczos algorithm, the orthogonal transformation matrix L is computed as $L = [\phi_1 \phi_2 \cdots \phi_n \cdots]$. Because of the construction of ϕ_1, it is easy to show that

$$G_{\alpha j,\alpha j}(Z) = \tilde{G}_{11}(Z). \quad (21)$$

The above process can be repeated to compute all the diagonal entries of G, i.e., for a given starting Lanczos state ϕ_1, the first n levels of the RCs a_l, $l=1,\ldots,n$, and b_l, $l=2,\ldots,n$, are first calculated by the Lanczos algorithm. Then, a_∞, b_∞, and the SRT function $t(Z)$ are computed. The first diagonal entry of the modified GF matrix, $\tilde{G}_{11}(Z)$, can be calculated by Eq. (17), which is identical to the desired diagonal entry of the original phonon GF matrix, $G_{\alpha j,\alpha j}(Z)$. Since only the first n (which is far less than N and does not depend on N) recursion levels are calculated, the recursion technique is an $O(N)$ method.

D. Local mechanical properties

Using the local Helmholtz free energy defined in Eq. (6), the local constitutive relation for mechanical analysis of nanostructures is given by

$$\mathbf{S}_{ij}(\mathbf{x}_\alpha) = \partial W_A^\alpha / \partial \mathbf{E}_{ij}, \quad i,j = 1,2,3, \quad (22)$$

where $\mathbf{S}_{ij}(\mathbf{x}_\alpha)$ is the second Piola-Kirchhoff stress tensor at position $\mathbf{x}_\alpha$, W_A^α is the Helmholtz free energy density of atom α which is defined by $W_A^\alpha = A_\alpha/\Omega_\alpha$, Ω_α is the volume of atom α in the initial configuration, and $\mathbf{E}$ is the Green-Lagrange strain tensor. The elastic constants for each atom position are given by[20]

$$\mathbf{C}_{ijkl}(\mathbf{x}_\alpha) = \frac{\partial^2 W_A^\alpha}{\partial \mathbf{E}_{ij} \partial \mathbf{E}_{kl}} - \frac{\partial^2 W_A^\alpha}{\partial \mathbf{E}_{ij} \partial \xi_m} \left(\frac{\partial^2 W_A^\alpha}{\partial \xi_m \partial \xi_n} \right)^{-1} \frac{\partial^2 W_A^\alpha}{\partial \xi_n \partial \mathbf{E}_{kl}}, \quad (23)$$

$$i,j,k,l,m,n = 1,2,3,$$

where $\mathbf{C}_{ijkl}(\mathbf{x}_\alpha)$ is the elastic constant tensor for atom α, and ξ are the additional inner displacements for a complex crystal structure such as diamond silicon. Due to the cubic symmetry of unstrained silicon, the pairs ij and kl in $\mathbf{C}_{ijkl}$ can be replaced by a single index p in the Voigt notation: $ij=11 \rightarrow p=1$, $ij=22 \rightarrow p=2$, and $ij=12$ or $ij=21 \rightarrow p=4$. Thus the three independent elastic constants for unstrained silicon with cubic symmetry are $\mathbf{C}_{11}$, $\mathbf{C}_{12}$, and $\mathbf{C}_{44}$. The derivatives of the Helmholtz free energy density with respect to the deformation parameters (i.e., $\mathbf{E}$ and ξ) are given by

$$\frac{\partial W_A^\alpha}{\partial \mathbf{v}} = \frac{1}{\Omega_\alpha} \left[\frac{\partial U_\alpha}{\partial \mathbf{v}} + k_B T \int_0^{\omega_{\max}} \ln\left(2 \sinh \frac{\hbar\omega}{2k_B T} \right) \frac{\partial n(\omega, \mathbf{x}_\alpha)}{\partial \mathbf{v}} d\omega \right], \quad (24)$$

where $\mathbf{v}$ can be replaced by $\mathbf{E}$ or ξ. The derivatives of the LPDOS can be obtained from the derivatives of the GF,

$$\frac{\partial n(\omega, \mathbf{x}_\alpha)}{\partial \mathbf{v}} = 2\omega \left(-\frac{1}{\pi} \lim_{\epsilon \rightarrow 0^+} \mathrm{Im} \sum_{j=1}^{3} \frac{\partial G_{\alpha j,\alpha j}(\omega^2 + i\epsilon)}{\partial \mathbf{v}} \right). \quad (25)$$

In the recursion technique, since the GF is expressed as a continued fraction and only the RCs a_l and b_l are a function of the deformation parameters, explicit expressions for the derivatives of the GF can be easily derived by using the chain rule. The calculation of these derivatives is presented in the Appendix.

III. SILICON SURFACE MODELS

In this work, we refer to ideal surfaces as the Si{001} surfaces (with dangling bonds). In addition to ideal surfaces we also consider reconstructed and hydrogen passivated reconstructed surfaces. The reconstruction of the Si{001} surfaces has previously been systematically examined using both classical potentials and *ab initio* calculations, and most calculations agree on the essentials of the Si{001} (2×1) reconstruction with the dimer bond along the $\langle 110 \rangle$ direction.[27–29] The periodicity of (2×1) is explained by the time average of the thermal flipflop motion of asymmetric dimmers on the Si{001} surfaces.[30,31] Moreover, for a hydrogen passivation of one monolayer, the surface retains a (2×1) reconstruction with hydrogen atoms terminating the dangling bonds of silicon. The ideal Si{001} surfaces, the (2×1)-reconstructed Si{001} surfaces, and the monolayer-hydrogen-passivated (2×1)-reconstructed Si{001} surfaces are studied in this work. These three configurations of the silicon surfaces are shown in Fig. 1. For both bulk silicon and the Si{001} surfaces, the Tersoff interatomic potential model[7] is used to approximate the Si-Si covalent bond interactions. For Si-H interactions, the empirical interatomic potential proposed in Ref. 34 is adopted in this work, since this extended version of the Tersoff potential has been tested successfully for its accuracy in decribing the Si-H system in solid form.[35,36] Note that the Tersoff potential gives a Si-Si dimer bond length of 2.37 Å. When a monolayer of hydrogen atoms are added on the (2×1) reconstructed Si{001} surfaces, the Si-Si dimer bond length increases to 2.43 Å, as shown in Fig. 1. For the real Si{001} surfaces, there exist steps, which belong to a generic defect class, line defects.[32,33] In this paper, we do not consider the existance of the steps on the silicon surfaces, and neglect the effect of the steps on the phonon structures, thermodynamic and mechanical properties of silicon nanowires.

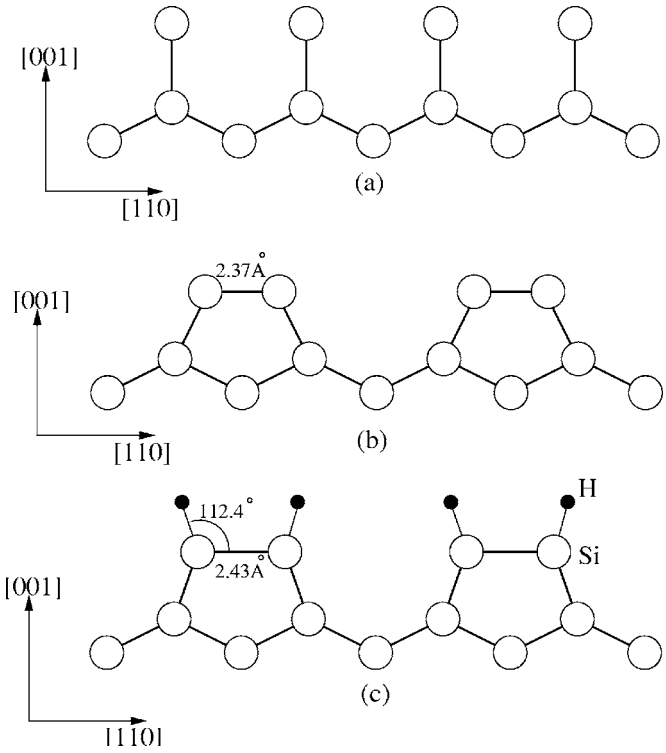

FIG. 1. The different silicon surfaces. (a) The ideal Si(001) surface, (b) the Si(001) surface with a (2×1) reconstruction, and (c) the (2×1)-reconstructed Si(001) surface with monolayer-hydrogen passivation.

IV. RESULTS AND DISCUSSION

A. LPDOS of bulk silicon and nanoscale silicon structures

In the quasiharmonic approximation, the elements of the mass-weighted force constant matrix $\hat{\Phi}$ are a function of the lattice constant a, the strain tensor $\mathbf{E}$, and the inner displacement ξ. Therefore, the LPDOS $n(\omega,\mathbf{x}_\alpha)$ and the Helmholtz free energy are also a function of a, $\mathbf{E}$, and ξ. For a given temperature T, the lattice constant a is first determined on the unstrained bulk silicon crystal by minimizing the Helmholtz free energy, i.e., by solving the equation $(\partial A/\partial a)_T=0$. The expression for the derivative of the Helmholtz free energy with respect to lattice constant a can be easily obtained from Eqs. (24) and (25) and the expressions given in the Appendix (by replacing $\mathbf{v}$ with a in the expressions in the Appendix). For the calculation of the mass-weighted force constant matrix, we use the analytical expressions, i.e., the second derivatives of the Tersoff potential for Si-Si interactions and Tersoff-type potential for Si-H interactions with respect to the atomic displacements. The analytical expressions for the derivatives of the Tersoff potential are given in Ref. 12. The expressions for the derivatives of the Tersoff-type potential for Si-H interactions are derived by following the same steps and are not provided here for the sake of brevity.

Figure 2 shows the computed lattice constant as a function of temperature by using the quasiharmonic phonon GF approach with different recursion levels (QHMG-n, where n represents the recursion level). The results from QHMK, LQHM, and MD simulations are also included in the figure

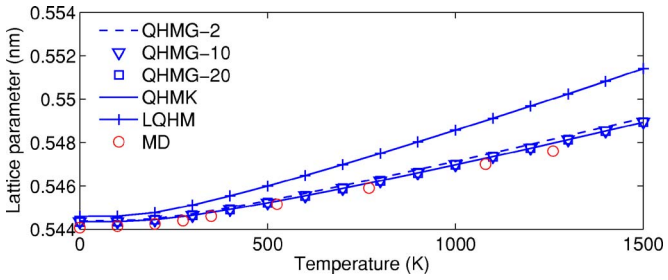

FIG. 2. (Color online) The lattice constant for Tersoff silicon at different temperatures. Results from QHMG-n are compared with those from QHMK, LQHM, and molecular dynamics (MD) simulations (MD data are from Ref. 39).

for comparison. Once the lattice constant a at the given temperature is computed, all the phonon structures can be easily obtained. For bulk silicon at 300 K, Fig. 3 shows a comparison of LPDOS between QHMK and QHMG-n by using Tersoff interatomic potential. Note that the LPDOS for the LQHM model is a δ-function located at $\omega=11$ THz. From the results on lattice constant and LPDOS for bulk silicon, we find that the calculation with 20 recursion levels results in a very good approximation.

Next, we calculate the LPDOS for a silicon nanowire consisting of $100\times5\times5$ unit cells, as shown in Fig. 4. We adopt three surface configurations as discussed in Sec. III to end the nanowire. For the preparation of the silicon nanowire with different surface configurations, we first generate the silicon diamond structure by using the lattice constant of the Tersoff silicon, which is 5.432 Å. Then the (2×1)-reconstructed surfaces and the hydrogen-terminated surfaces are formed by using the parameters given in Refs. 34 and 36. Then we use MD simulations to relax the structure (no external loads applied) and obtain the equilibrium geometry of the nanowire. For the nanowire with ideal surfaces, the interested atom positions are exactly as shown in Fig. 4, and the surface atoms (1 and 12) have only two bonds. For the nanowire with (2×1)-reconstructed surfaces, the positions of atoms 1 and 12 are slightly different, and atoms 1 and 12 have three bonds where the new bonds are generated from the surface reconstruction. For the nanowire with (2×1)-reconstructed surfaces with hydrogen passivation, the positions of atoms 1 and 12 are also slightly different and atoms 1 and 12 have four bonds. Figure 5 gives the

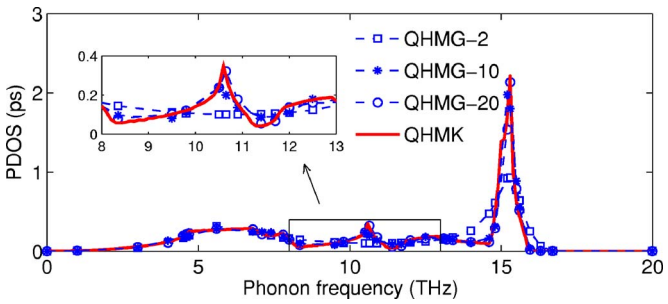

FIG. 3. (Color online) LPDOS for bulk Tersoff silicon: comparison between QHMK and QHMG-n at 300 K. Note that the LPDOS from LQHM is a δ function located at $\omega=11$ THz.

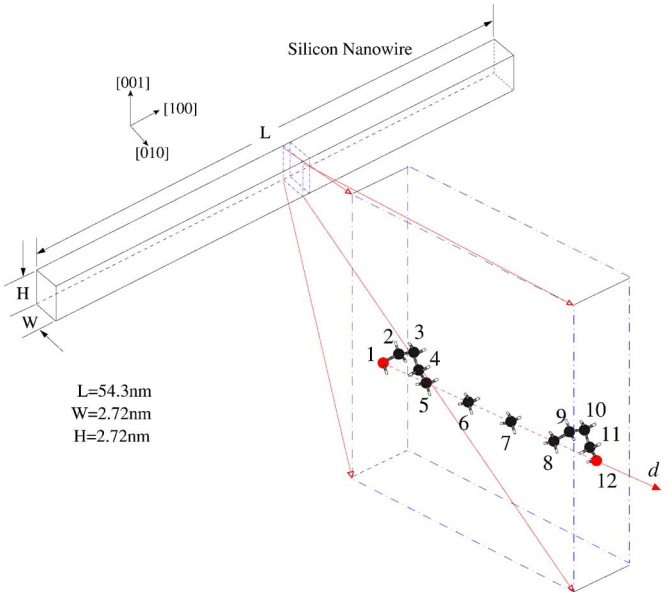

FIG. 4. (Color online) The silicon nanowire ($100\times5\times5$ unit cells). The atoms of interest (atoms 1 to 12) are shown. For the nanowire with ideal surfaces, the atom positions are exactly as shown in the figure. For the nanowire with (2×1)-reconstructed surfaces and (2×1)-reconstructed surfaces with hydrogen passivation, the positions of atoms 1 and 12 are slightly different.

LPDOS for different atom positions in the nanowire (see Fig. 4 for the locations of the atoms) at 300 K. From Fig. 5(a), we find that, for the surface atoms, the acoustic phonons have lower frequencies. This is because the atoms on the surface have fewer bonds (compared to bulk) and this leads to the softening of the phonon frequency. Moreover, from Fig. 5(a), we find that the acoustic phonons are shifted to the right (toward higher frequencies) for reconstructed surfaces. The reason is that the surface reconstruction and hydrogen passivation generate more bonds for the surface atoms. However, for the reconstructed surfaces with hydrogen passivation, even though the surface silicon atoms also have four bonds (the same number as for bulk silicon atoms), their LPDOS are still quite different from the LPDOS of bulk silicon atoms. This is because Si-H interactions are weaker than the Si-Si interactions. A new peak is observed at about 57 THz for the surface silicon atom in the nanowire with hydrogen passivation on the surfaces as shown in Fig. 5(a). This high frequency is due to the Si-H bond stretching vibrations [e.g., the stretching vibrational frequency for SiH molecule is 61 THz (Ref. 34)]. From Figs. 5(b) and 5(c), we observe that for the atom positions inside the surface, the LPDOS are quite similar to that of the bulk. The highest peak (at about 57 THz) disappears for both atoms 2 and 5. The phonons in the range of 15–18 THz are shifted toward higher frequencies for atom 2, due to the effect of the Si-H bond on the surface. This effect, however, is not seen for atom 5, where the LPDOS is almost the same as that of the bulk, for all three silicon nanowires.

B. Local thermal properties

After the LPDOSs are calculated, the Helmholtz free energy can be obtained from Eq. (6). All other thermodynamic properties can then be obtained easily. Figure 6 shows the local thermodynamic properties (Helmholtz free energy, internal energy, vibrational energy, kinetic energy, entropy, and heat capacity) as a function of the atom positions.

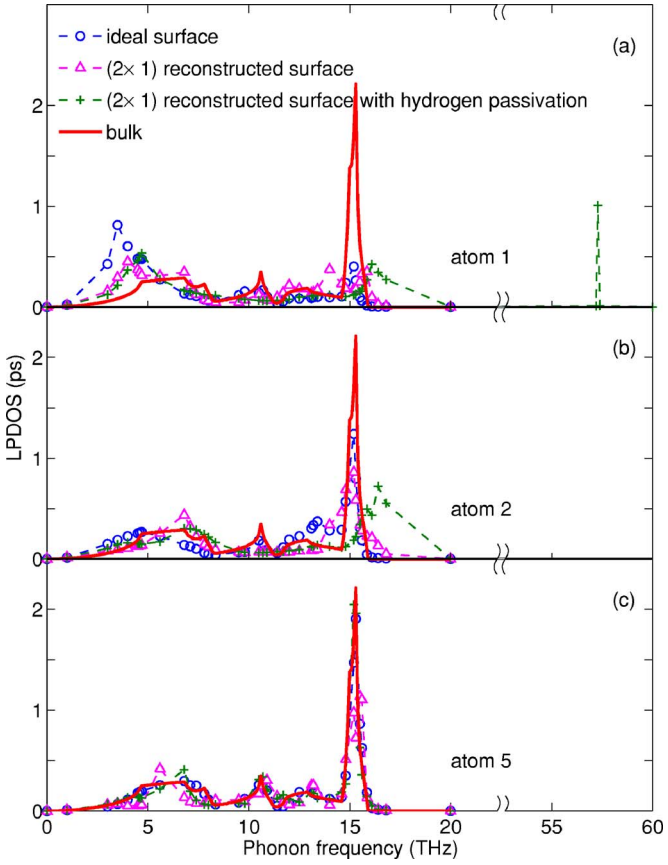

FIG. 5. (Color online) The LPDOS calculated by QHMG-20 for different atom positions in the silicon nanowire shown in Fig. 4 with ideal surface (circles with dashed line), (2×1) reconstruction (triangles with dashed line), and (2×1) reconstruction with hydrogen passivation (plus with dashed line) at 300 K. The QHMK result for bulk silicon (solid line) is also given for comparison.

From Figs. 6(a) and 6(b), we find that the free energy and the internal energy for surface atoms are higher than those for interior atoms, for silicon nanowires with ideal Si{001} surfaces and with (2×1) surface reconstructions. For the silicon nanowire with (2×1) surface reconstruction and hydrogen passivation, the free energy and internal energy for the surface silicon atoms are lower than those for the interior atoms. This is because the static energy is the dominant contribution to the Helmholtz free energy and internal energy, and the presence of hydrogen atoms on the (2×1)-reconstructed Si{001} surfaces lowers the static potential energy as the bond energy for Si-H is lower than the Si-Si bond energy [e.g., the bond energy for SiH molecule is −3.1 eV, which is lower than the bond energy for Si_2 molecule, −2.66 eV (Ref. 34)].

Figures 6(c) and 6(d) indicate that the vibrational energy and the kinetic energy of the surface atoms for silicon nanowire with ideal Si{001} surfaces are lower than those for the interior atoms. The decrease in the vibrational and kinetic energies of the surface atoms when compared to the interior

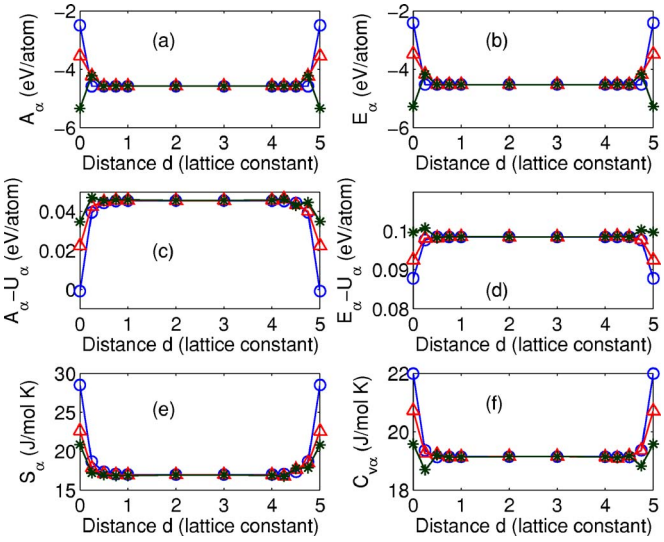

FIG. 6. (Color online) Variation of thermodynamic properties [(a) Helmholtz free energy, (b) internal energy, (c) vibrational energy, (d) kinetic energy, (e) entropy, (f) heat capacity] with different atom positions (denoted by the distance from the rear surface, d) computed by QHMG-20 for the silicon nanowire shown in Fig. 4 with three surface configurations: ideal surface (circles with solid line), (2×1) reconstruction (triangles with solid line), and (2×1) reconstruction with hydrogen passivation (stars with solid line). $T=300$ K.

atoms is due to the phonon softness on the surface, as described in Sec. IV A. Since the vibrational energy and the kinetic energy are a measure of the vibrational movement in the system, low-frequency phonons result in a lower vibrational energy and kinetic energy for the surface atoms. Moreover, by comparing the results for all the three surfaces in Figs. 6(c) and 6(d), we find that the surface reconstruction first increases the vibrational and kinetic energy, and the introduction of hydrogen atoms on the reconstructed surface further increases the vibrational and the kinetic energies. The reason is, as described in Sec. IV A, due to the surface reconstruction and hydrogen passivation, new Si-Si and Si-H bonds are formed, and the low-frequency phonons are shifted toward higher frequencies. Since the high-frequency phonons have higher energy, the shift of the low-frequency phonons results in the increase of the vibrational and kinetic energies for the atoms near the surfaces.

Figure 6(e) shows that the entropy of the surface atoms is higher compared to the interior atoms. This is because the entropy is a measure of the disorder of the system, and the surface atoms increase the disorder of the system. Since the surface reconstruction forms new Si-Si bonds on the surfaces, the disorder of the system is decreased and the entropy is thus decreased. The introduction of hydrogen atoms on the reconstructed surfaces forms new Si-H bonds and the disorder of the system is further decreased. Therefore, the silicon nanowire with (2×1) surface reconstruction and hydrogen passivation has the lowest entropy for those atom positions near the surfaces, as shown in Fig. 6(e). From Fig. 6(f), we find that the heat capacity of the surface atoms is also higher compared to the interior atoms for the silicon nanowire with ideal Si{001} surfaces, and the surface reconstruction and hydrogen passivation decrease the heat capacities.

C. Mechanical properties

The local elastic properties for the different atom positions in the silicon nanowire are calculated by Eq. (23). Figure 7 shows the variation of the elastic properties with atom positions at room temperature ($T=300$ K) for the silicon nanowire with ideal Si{001} surfaces. We find that the elastic constants for the atoms near the surface are smaller than those farther way from the surface. The variation of the elastic constants for interior atoms is small ($\Delta\mathbf{C}_{11}<0.5\%$, $\Delta\mathbf{C}_{12}<0.7\%$, and $\Delta\mathbf{C}_{44}<0.3\%$). Thus, the effect of the surface on the elastic constants of the interior atoms is negligible. The calculation of the elastic constants for the surface atoms (i.e., atoms 1 and 12) is a nontrivial task as the Cauchy-Born rule is not applicable for the surface atoms. To investigate the surface effect on the elastic properties, we calculate the average elastic constants for a silicon nanowire with a length of 44 nm and various square cross-sectional areas. The averaged elastic constants are calculated by differentiating the total Helmholtz free energy with respect to $\mathbf{E}$ and ξ. Figure 8(a) shows the elastic constants as a function of the nanowire cross-sectional area at $T=300$ K. Note that the cubic symmetry of the bulk silicon crystal lattice breaks down due to the finite size along the [010] direction and this results in $\mathbf{C}_{1111}\neq\mathbf{C}_{2222}$, as shown in Fig. 8(a). The Young's modulus along the [100] direction can be obtained by $E_{[100]}=\mathbf{C}_{1111}-2\mathbf{C}_{1122}^2/(\mathbf{C}_{2222}+\mathbf{C}_{1122})$. Figure 8(b) shows the Young's modulus along the [100] direction as a function of the nanowire cross-sectional area at $T=300$ K. For comparison, the Young's modulus from stretch tests with MD simulations at constant temperature[4] is also shown in Fig. 8(b). From these results we can conclude that, when the cross-sectional area is larger than $10\sim15$ nm^2, the Young's modulus of the silicon nanowire is same as that of the bulk silicon. For the silicon nanowire with ideal Si{001} surfaces, the deformation of the atoms in the surface region can be approximated as homogeneous and the calculation of the averaged elastic constant is possible. However, for the silicon nanowires with surface reconstruction and hydrogen passivation, surface region has a curvature. The use of the standard Cauchy-Born rule for atoms in the curved surfaces can be inaccurate. Recently the standard Cauchy-Born rule has been extended for nanostructures with curvatures e.g. carbon nanotubes.[37,38] The application of the extended Cauchy-Born rule for surface reconstructions in silicon is not a trivial task and we leave this topic for future work.

V. CONCLUSIONS

In conclusion, we have investigated the local thermodynamic and mechanical properties of silicon nanostructures using local phonon GF method and have established the constitutive relation which plays a key role in finite temperature multiscale analysis of nanostructures. For silicon nanowires with ideal Si{001} surfaces, with (2×1) surface reconstruction, and with surface reconstruction and hydrogen passiva-

tion, we calculate the phonon structures and local thermal properties. For the silicon nanowire with ideal surfaces, the local elastic constants and the averaged elastic properties are computed and the averaged elastic constants are compared with molecular dynamics simulation results. The calculations on the local thermal and mechanical properties show that the surface effects for silicon nanostructures are quite localized.

ACKNOWLEDGMENTS

This work is supported by the National Science Foundation under Grants No. 0103447, No. 0228390, No. 0403020, and No. 0519920.

APPENDIX: CALCULATION OF THE DERIVATIVES OF THE PHONON GF IN A RECURSION SCHEME

Consider the calculation of the diagonal entries of the phonon GF given by Eqs. (14) and (21). Following the standard procedure of matrix inversion, Eq. (21) can be rewritten as

$$G_{\alpha j,\alpha j}(Z) = \tilde{G}_{11} = \frac{D_1}{D_0} = \frac{1}{\tilde{D}_0}, \tag{A1}$$

where D_0 is the determinant of $Z\mathbf{I}-\Phi^{TD}$, D_1 is the determinant of $Z\mathbf{I}-\Phi_1^{TD}$, and Φ_1^{TD} is a submatrix formed by omitting the first row and the first column of the tridiagonal matrix Φ^{TD}. By using the Laplace expansion for the first row of $Z\mathbf{I}-\Phi^{TD}$, we have

$$D_0 = (Z-a_1)D_1 - b_2^2 D_2, \tag{A2}$$

where D_2 is the determinant of $Z\mathbf{I}-\Phi_2^{TD}$, and Φ_2^{TD} is a submatrix formed by omitting the first row and the first column of the tridiagonal matrix Φ_1^{TD}. Generalizing the above equation, we have

$$D_l = (Z-a_{l+1})D_{l+1} - b_{l+2}^2 D_{l+2}, \quad l=0,1,\ldots,n-1. \tag{A3}$$

By defining $\tilde{D}_l = D_l/D_{l+1}$, Eq. (A3) can be rewritten as

$$\tilde{D}_l = (Z-a_{l+1}) - b_{l+2}^2/\tilde{D}_{l+1}, \quad l=0,1,\ldots,n-1. \tag{A4}$$

For the SRT terminator, we have

$$\tilde{D}_n = \frac{1}{t(Z)}. \tag{A5}$$

Thus, from Eq. (A1) the first derivatives of the phonon GF with respect to any deformation parameter $\mathbf{v}$ can be written as

$$\frac{\partial G_{\alpha j,\alpha j}(Z)}{\partial \mathbf{v}} = -\frac{1}{\tilde{D}_0^2}\frac{\partial \tilde{D}_0}{\partial \mathbf{v}}, \tag{A6}$$

and this can be calculated by using a recursion scheme as

$$\frac{\partial \tilde{D}_l}{\partial \mathbf{v}} = -\frac{\partial a_{l+1}}{\partial \mathbf{v}} - \frac{2b_{l+2}}{\tilde{D}_{l+1}}\frac{\partial b_{l+2}}{\partial \mathbf{v}} + \frac{b_{l+2}^2}{\tilde{D}_{l+1}^2}\frac{\partial \tilde{D}_{l+1}}{\partial \mathbf{v}}, \quad l=0,1,\ldots,n-1, \tag{A7}$$

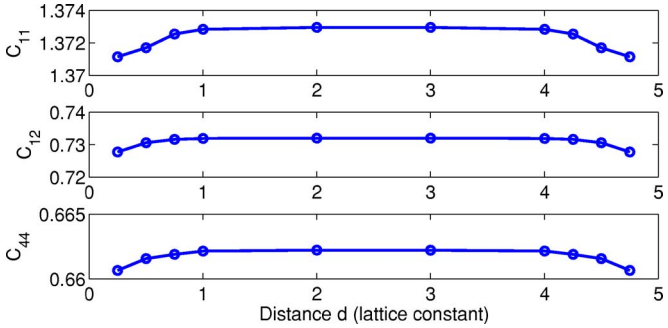

FIG. 7. (Color online) Variation of elastic constants (in Mbars) with different atom positions (denoted by the distance from the rear surface, d) for the silicon nanowire with ideal surfaces shown in Fig. 4. $T=300$ K.

$$\frac{\partial \tilde{D}_n}{\partial \mathbf{v}} = -\frac{1}{t^2(Z)}\frac{\partial t(Z)}{\partial \mathbf{v}}, \tag{A8}$$

$$\frac{\partial t(Z)}{\partial \mathbf{v}} = -\frac{t(Z)}{b_\infty}\frac{\partial b_\infty}{\partial \mathbf{v}} + \frac{1}{b_\infty}\left(1+\frac{i\eta(Z)}{\sqrt{1-\eta^2(Z)}}\right)\frac{\partial \eta(Z)}{\partial \mathbf{v}}, \tag{A9}$$

$$\frac{\partial \eta(Z)}{\partial \mathbf{v}} = -\frac{1}{b_\infty}\left(\frac{1}{2}\frac{\partial a_\infty}{\partial \mathbf{v}} + \eta(Z)\frac{\partial b_\infty}{\partial \mathbf{v}}\right). \tag{A10}$$

To calculate the derivatives of the RCs which are needed in Eqs. (A7)–(A10), consider the Lanczos algorithm, which is given by Eq. (20) and its related equations, and this results in the following equations:

$$\frac{\partial \tilde{\phi}_{l+1}}{\partial \mathbf{v}} = \left(\frac{\partial \hat{\Phi}}{\partial \mathbf{v}} - \frac{\partial a_l}{\partial \mathbf{v}}\mathbf{I}\right)\phi_l + (\hat{\Phi}-a_l\mathbf{I})\frac{\partial \phi_l}{\partial \mathbf{v}} - \frac{\partial b_l}{\partial \mathbf{v}}\phi_{l-1} - b_l\frac{\partial \phi_{l-1}}{\partial \mathbf{v}}, \tag{A11}$$

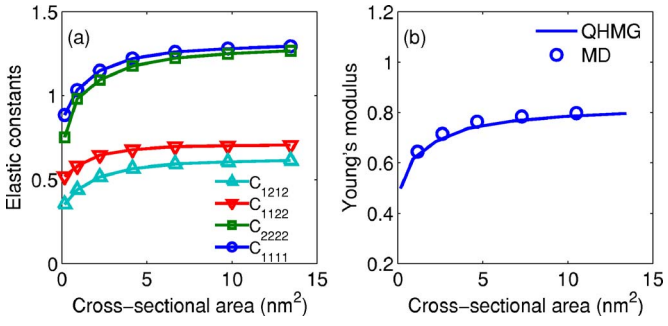

FIG. 8. (Color online) (a) Variation of elastic constants (in Mbars) with cross-sectional area for the silicon nanowire with ideal surfaces. (b) Variation of Young's modulus (in Mbars) along [100] direction with cross-sectional area. The length of the silicon nanowire (with ideal surfaces) is chosen as 44 nm, which is large enough to eliminate the surface effect in the length direction. $T=300$ K.

$$\frac{\partial a_{l+1}}{\partial \mathbf{v}} = 2\frac{\partial \tilde{\phi}_{l+1}^T}{\partial \mathbf{v}}\hat{\Phi}\tilde{\phi}_{l+1} + \tilde{\phi}_{l+1}^T\frac{\partial \hat{\Phi}}{\partial \mathbf{v}}\tilde{\phi}_{l+1}, \tag{A12}$$

$$\frac{\partial b_{l+1}}{\partial \mathbf{v}} = \frac{1}{b_{l+1}}\frac{\partial \tilde{\phi}_{l+1}^T}{\partial \mathbf{v}}\tilde{\phi}_{l+1}, \tag{A13}$$

$$\frac{\partial \phi_{l+1}}{\partial \mathbf{v}} = -\frac{1}{b_{l+1}^2}\frac{\partial b_{l+1}}{\partial \mathbf{v}}\tilde{\phi}_{l+1} + \frac{1}{b_{l+1}}\frac{\partial \tilde{\phi}_{l+1}}{\partial \mathbf{v}}, \tag{A14}$$

$$\frac{\partial a_\infty}{\partial \mathbf{v}} = \frac{1}{n}\sum_{l=1}^{n}\frac{\partial a_l}{\partial \mathbf{v}}, \tag{A15}$$

$$\frac{\partial b_\infty}{\partial \mathbf{v}} = \frac{1}{n}\sum_{l=2}^{n+1}\frac{\partial b_l}{\partial \mathbf{v}}. \tag{A16}$$

The second derivatives can be derived in the same manner and these are not given here for the sake of brevity.

[1] Y. Cui and C. M. Liber, Science **291**, 851 (2001).
[2] H. G. Craighead, Science **290**, 1532 (2000).
[3] M. Paulose, C. A. Grimes, O. K. Varghese, and E. C. Dickey, Appl. Phys. Lett. **81**, 153 (2002).
[4] Z. Tang, Y. Xu, G. Li, and N. R. Aluru, J. Appl. Phys. **97**, 114304 (2005).
[5] S. Wei, C. Li, and M. Y. Chou, Phys. Rev. B **50**, 14587 (1994).
[6] F. H. Stillinger and T. A. Weber, Phys. Rev. B **31**, 5262 (1985).
[7] J. Tersoff, Phys. Rev. B **38**, 9902 (1988).
[8] J. M. Dickey and A. Paskin, Phys. Rev. **188**, 1407 (1969).
[9] A. A. Maradudin, E. W. Montroll, G. H. Weiss, and I. P. Ipatova, *Theory of Lattice Dynamics in the Harmonic Approximation* (Academic Press, New York, 1971).
[10] R. LeSar, R. Najafabadi, and D. J. Srolovitz, Phys. Rev. Lett. **63**, 624 (1989).
[11] H. Zhao, Z. Tang, G. Li, and N. R. Aluru, J. Appl. Phys. **99**, 064314 (2006).
[12] Z. Tang, H. Zhao, G. Li, and N. R. Aluru, Phys. Rev. B **74**, 064110 (2006).
[13] R. Haydock, V. Heine, and M. J. Kelly, J. Phys. C **5**, 2845 (1972).
[14] P. E. Meek, Philos. Mag. **33**, 897 (1976).
[15] M. J. Kelly, Solid State Phys. **35**, 295 (1980).
[16] M. Born and K. Huang, *Dynamical Theory of Crystal Lattices* (Clarendon, Oxford, 1954).
[17] E. B. Tadmor, G. S. Smith, N. Bernstein, and E. Kaxiras, Phys. Rev. B **59**, 235 (1999).
[18] N. W. Ashcroft and N. D. Mermin, *Solid State Physics* (Harcourt, 1976).
[19] J. Li and S. Yip, Phys. Rev. B **56**, 3524 (1997).
[20] D. C. Wallace, *Thermodynamics of Crystals* (John Wiley & Sons, New York, 1972).
[21] E. N. Economou, *Green's Functions in Quantum Physics* (Springer-Verlag, Berlin, 1983).
[22] H. S. Wall, *Analytical Theory of Continued Fractions* (Van Nostrand-Reinhold, Princeton, NJ, 1948).
[23] A. Jennings and J. J. McKeown, *Matrix Computation* (John Wiley & Sons, New York, 1992).
[24] A. P. Horsfield, A. M. Bratkovsky, M. Fearn, D. G. Pettifor, and M. Aoki, Phys. Rev. B **53**, 12694 (1996).
[25] D. G. Pettifor and D. L. Weaire, *The Recursion Method and Its Applications* (Springer-Verlag, Berlin, 1985).
[26] C. Lanczos, J. Res. Natl. Bur. Stand. **45**, 255 (1950).
[27] R. M. Tromp, R. J. Hamers, and J. E. Demuth, Phys. Rev. Lett. **55**, 1303 (1985).
[28] S. Ihara, S. L. Ho, T. Uda, and M. Hirao, Phys. Rev. Lett. **65**, 1909 (1990).
[29] I. P. Batra, Phys. Rev. B **41**, 5048 (1990).
[30] J. Dabrowski and H. J. Mussig, *Silicon Surfaces and Formation of Interfaces* (World Scientific, Singapore, 2000).
[31] T. Shirasawa, S. Mizuno, and H. Tochihara, Phys. Rev. Lett. **94**, 195502 (2005).
[32] R. M. Tromp and M. C. Reuter, Phys. Rev. B **47**, 7598 (1993).
[33] L. Zhong, A. Hojo, Y. Aiba, and K. Chaki, Appl. Phys. Lett. **68**, 1823 (1996).
[34] M. V. Ramana Murty and H. A. Atwater, Phys. Rev. B **51**, 4889 (1995).
[35] T. Hawa and M. R. Zachariah, Phys. Rev. B **69**, 035417 (2004).
[36] U. Hansen and P. Vogl, Phys. Rev. B **57**, 13295 (1998).
[37] M. Arroyo and T. Belytschko, Phys. Rev. B **69**, 115415 (2004).
[38] K. Chandraseker, S. Mukherjee, and Y. X. Mukherjee, Int. J. Solids Struct. **43**, 7128 (2006).
[39] L. J. Porter, S. Yip, M. Yamaguchi, H. Kaburaki, and M. Tang, J. Appl. Phys. **81**, 96 (1997).